Comparison Between Trion and Exciton Electronic Properties in CdSe and PbS Nanoplatelets

David F. Macias-Pinilla,[†,‡] Josep Planelles,[†] Iván Mora-Seró,[‡] and Juan I. Climente[*,†]

†*Departament de Química Física i Analítica, Universitat Jaume I, Av. Sos Baynat, s/n, 12071 Castelló, Spain*

‡*Institute of Advanced Materials (INAM), Universitat Jaume I, Av. Sos Baynat, s/n, 12071 Castelló, Spain*

E-mail: climente@uji.es

Abstract

The optoelectronic properties of metal chalcogenide colloidal nanoplatelets are often interpreted in terms of excitonic states. However, recent spectroscopic experiments evidence the presence of trion states, enabled by the slow Auger recombination in these structures. We analyze how the presence of an additional charge in trions modifies the emission energy and oscillator strength as compared to neutral excitons. These properties are very sensitive to dielectric confinement and electronic correlations, which we describe accurately using image-charge and variational Quantum Monte Carlo methods in effective mass Hamiltonians. We observe that the giant oscillator strength of neutral excitons is largely suppressed in trions. Both negative and positive trions are redshifted with respect to the exciton, and their emission energy increases with increasing dielectric mismatch between the platelet and its surroundings, which is a consequence of the self-energy potential. Our results are consistent with experiments in the literature, and assess on the validity of previous theoretical approximations.

Introduction

The outstanding optical features of semiconductor colloidal nanoplatelets (NPLs) makes them a broad target of study and application in devices.[1–4] As compared to colloidal quantum dots, the quasi-2D nature of NPLs conveys several distinct properties of interest, including precisely controllable thickness –which enables narrow emission linewidths–, large absorption cross-sections and bright luminescence resulting from the giant oscillator strength effect.[2–4] Several efforts have been carried out in synthesis methods to control the morphology, dimensions and composition, as well as in characterization of the subsequent optoelectronic properties.[4–7] In parallel, theoretical models have been developed to understand the underlying electronic structure. In most cases, such models focus on neutral excitons,[8–22] which is typically the dominant emitting species in colloidal nanocrystals.

There is however increasing evidence that the emission spectrum of core-only and core/shell

CdSe NPLs at low temperatures has a significant contribution from charged excitons (trions).[23–29] The formation of radiative trions is enabled by the higher dimensionality of NPLs as compared to nanocrystals, which slows down Auger relaxation processes.[30–33] Trions are of high technological interest for optoelectronic applications. The spin-zero configuration in one of the bands suppresses the electron-hole exchange interaction, and hence the optically dark ground state observed in the fine structure of neutral excitons, which is convenient for efficient luminescence.[25] They also enable two-color emission through shake-up processes[34] –which are particularly strong in colloidal NPLs[26,35]–, provide a photoresponsive system for chemical sensing through surface adsorption[23] and form a natural two-level quantum system for quantum information applications.[28]

Understanding how the electronic structure of trions differs from that of excitons is a prerequesite for rational design of applications. In a recent work, Peng *et al.* analyzed the emission spectra of exciton and trion states in CdSe NPLs with 4.5 monolayers core thickness surrounded by thin CdS/ZnS shells.[28] By comparing time-resolved photoluminescence data with tight-binding simulations, which accounted for electronic correlations using a configuration interaction (CI) approach, they assigned the observed spectral peaks to neutral excitons and negative trions. The latter showed binding energies of about 10.5 meV, and similar oscillator strength to that of the exciton band edge transition. In parallel, Ayari *et al.* investigated the negative trion emission spectra in CdSe core-only NPLs with the same thickness, but varying lateral dimensions.[29] They observed stronger trion binding energies, widely modulated by the lateral confinement (18-36 meV). By comparing time-integrated photoluminescence data with rate equation models and effective mass-CI calculations of the electronic structure, they inferred that the oscillator strength of trions is one order of magnitude weaker than that of the excitons. The seemingly contradicting conclusions in the two studies call for independent assessment.

To better understand how the photophyics of trions in NPLs differs from that of excitons, one must account for the fact that electronic correlations are particularly challenging

to model in these structures. Unlike quantum dots, NPLs lie in a Coulomb dominated, intermediate confinement regime,[13,14] where the strong electron-hole attraction –arising from dielectric confinement and the quasi-2D geometry– leads to small excitonic radii.[36] Such a short-range interaction makes CI calculations based on envelope wave functions miss correlation energy.[37,38] By contrast, the electron-electron (or hole-hole) repulsions in trions, which are also enhanced by the quasi-2D geometry and the dielectric confinement, are longer-ranged interactions and hence better captured by CI models. Conclusions about the balance between attractive and repulsive forces in these systems must be revisited using methods which account for both of them on equal footing.

In this work, we calculate the electronic structure of excitons and trions in colloidal NPLs using effective mass Hamiltonians which include electronic correlations though a variational Quantum Monte Carlo (VQMC) description. This method has been recently shown to outperform CI approaches in these systems.[39] We choose CdSe and PbS NPLs, which are systems of current interest for direct applications including solar cells,[40,41] photodetectors operating in the near infrared,[42] light-emitting diodes[43–45] and lasers.[46] We provide an overview on the differences between neutral excitons and trions, and examine some of the approximations used in earlier models, such as the description of dielectric confinement with Rytova-Keldysh (RK) potential and neglecting self-energy corrections.[29] We shall see that of both positive and negative trions are bound for typical NPL dimensions, with binding energies which (for CdSe) exceed room temperature thermal energy. The repulsions in trions lead to a moderate increase of the excitonic Bohr radius and induce a significant suppression of the oscillator strength as compared to neutral excitons. Similar to excitons, dielectric confinement leads to an overall increase of the trion emission energy.

Methods

We calculate exciton and trion ground state energies and wave functions closely following Ref. 39. Briefly, we solve effective mass Hamiltonians of the form:

$$H = \sum_{i=1}^{N_e} \hat{h}_e + \sum_{i=1}^{N_h} \hat{h}_h + \sum_{i=1}^{N_e}\sum_{j=1}^{N_h} V_c(\mathbf{r}_i, \mathbf{r}_j) + 1/2 \sum_{i=1}^{N_e}\sum_{j\neq i}^{N_e} V_c(\mathbf{r}_i, \mathbf{r}_j) + 1/2 \sum_{i=1}^{N_h}\sum_{j\neq i}^{N_h} V_c(\mathbf{r}_i, \mathbf{r}_j) + E_{gap}. \tag{1}$$

where N_e and N_h is the number of electrons and holes, while $\hat{h}_e$ and $\hat{h}_h$ are the corresponding single-particle Hamiltonians:

$$\hat{h}_i = \Big(\frac{\hat{\mathbf{p}}_\perp^2}{2m_{\perp,i}} + \frac{\hat{p}_z^2}{2m_{z,i}} + V \Big). \tag{2}$$

Here, $m_\perp$ and $\hat{\mathbf{p}}_\perp$ ($m_{z,i}$ and $\hat{p}_z^2$) are the in-plane (out-of-plane) effective mass and momentum operators, respectively. $V = V^{conf} + \Sigma$, is the single particle potential, with V^{conf} the spatial confinament potential –zero inside the cuboidal NPL, infinite outside it–, and Σ the self-energy potential arising from dielectric confinement. $V_c(\mathbf{r}_i, \mathbf{r}_j)$ are the Coulomb interaction terms and E_{gap} the bulk band gap.

Dielectric confinement is important in colloidal NPLs, owing to the strong mismatch between the inorganic NPL and the organic surroundings. Because the organic environment screens electric fields more weakly than the semiconductor lattice, it gives rise to enhanced Coulomb interactions.[9,10,13] We model this effect using image-charge (IC) expressions developed for finite-width quantum wells. Self-energy corrections (Σ) are included within the same formalism to account for the changes that individual carriers produce on their own dielectric environment.[47] In some instances, for the sake of comparison, the Coulomb enhancement arising from dielectric confinement is modeled using a RK potential instead, which is an approximation of the Coulomb potential for the limit case of a quantum well with zero thickness and static dielectric screening.[48]

To solve Hamiltonian (1), a variational trial wave function is defined for excitons:

$$\Psi_X(\mathbf{r_e}, \mathbf{r_h}, \sigma_e, \sigma_h) = N_X \, \Phi_e(\mathbf{r_e})\Phi_h(\mathbf{r_h})J(r_{eh}), \tag{3}$$

where N_X is the normalization constant, Φ_e and Φ_h are the envelope functions of non-interacting electron and hole, and $J(r_{eh}) = e^{-r_{eh}/r_B^X}$ is a Slater correlation factor, with r_{eh} the electron-hole separation and r_B^X the effective exciton Bohr radius, which is the variational parameter to optimize. For negative trions, the ground state involves double occupancy of the lowest electron orbital (associated to singlet spin) plus one hole. Then, a Slater-Jastrow trial wave function is used:

$$\Psi_{X^-}(\mathbf{r_{e_1}}, \mathbf{r_{e_2}}, \mathbf{r_{h_1}}, \sigma_{e_1}, \sigma_{e_2}, \sigma_{h_1}) = N_{X^-} \, \Phi_e(\mathbf{r_{e_1}})\Phi_e(\mathbf{r_{e_2}})\Phi_h(\mathbf{r_{h_1}})J(r_1, r_2, r_{12}). \tag{4}$$

Here, N_{X^-} the normalization factor and $J(r_1, r_2, r_{12}) = e^{-r_1/r_B^{X^-}} \; e^{-r_2/r_B^{X^-}} \; e^{\frac{br_{12}}{1+ar_{12}}}$ the Jastrow factor, with $r_1 = |\mathbf{r_{e_1}} - \mathbf{r_{h_1}}|$, $r_2 = |\mathbf{r_{e_2}} - \mathbf{r_{h_1}}|$ and $r_{12} = |\mathbf{r_{e_1}} - \mathbf{r_{e_2}}|$. In this case, $r_B^{X^-}$, b and a are the variational parameters to optimize. The first one is related to attractions and the others to repulsions. Analogous expressions are used for positive trions.

Variational optimization is carried out using a VQMC algorithm, with the freely available codes we developed in Ref. 39. Iterative Newton-Rhapson convergence is compared with sequential optimization of the variational parameters to avoid local minima. The optical recombination probability for the resulting wave functions can be estimated within the dipole approximation.[49] For a neutral exciton, the transition from $|\Psi_X\rangle$ to a vacuum state $|0\rangle$ is proportional to the electron-hole overlap:[13]

$$\tau_{X\to 0}^{-1} \propto 1/2 \, |\langle 0|\delta_{\mathbf{r_e},\mathbf{r_h}}|\Psi_X\rangle|^2 = \frac{1}{2}\left(\frac{N_X}{N_e \, N_h}\right)^2. \tag{5}$$

where N_i is the normalization constant of a single-particle orbital Φ_i, $N_e = N_h = \sqrt{8/(L_x L_y L_z)}$ in our particle-in-box functions, with L_x, L_y and L_z the NPL dimensions. The 1/2 factor

accounts for spin selection rules forbidding optical transitions in dark excitons. Notice we assume equal population of bright and dark exciton states, which is the case except for cryogenic temperatures, since the splitting between these states is under 6 meV.[25] For a negative trion, the transition from $|\Psi_X^-\rangle$ to an electron state $|\Psi_e\rangle = N_e\Phi_e(\mathbf{r_{e_1}})$ is proportional to:

$$\tau^{-1}_{X^-\to e} \propto \left|\langle\Psi_e|\delta_{\mathbf{r_{e_2}},\mathbf{r_{h_1}}}|\Psi_{X^-}\rangle\right|^2 = (N_e\, N_{X^-}\,\mathcal{I})^2, \tag{6}$$

with $\mathcal{I} = \int \Phi_e(\mathbf{r_{e_1}})^2\,\Phi_e(\mathbf{r_{e_2}})\,\Phi_h(\mathbf{r_{e_2}})\,e^{-r_{12}/r_B^{X^-}}\,e^{\frac{br_{12}}{1+ar_{12}}}\,d^3r_{e_1}\,d^3r_{e_2}$.

Results and Discussion

We investigate excitons and trions in CdSe and PbS NPLs with cubic crystal lattice. Material parameters are summarized in Table 1. For CdSe, we consider NPLs with 4.5 monolayer thickness ($L_z = 1.4$ nm), as in the samples measured in Refs. 28 and 29. For PbS, we choose a typical thickness of $7-8$ monolayers ($L_z = 2.0$ nm).[50] Unless otherwise stated, for both CdSe and PbS NPLs we consider an environmental dielectric constant due to the organic ligands of $\varepsilon_{out} = 2$.[9,51]

Table 1: Material parameters used in the calculations. ε_0 is the vacuum permittivity, m_0 is the free electron mass and a_0 stands for the lattice constant. The references indicate the data source.

Parameter	CdSe	PbS	Units
ε_{NPL}	10[52]	17[53]	ε_0
$m_{\perp,e}$	0.22[10]	0.27[21]	m_0
$m_{\perp,h}$	0.41[10]	0.19[21]	m_0
$m_{z,e}$	0.4[13]	0.29[21]	m_0
$m_{z,h}$	0.9[13]	0.25[21]	m_0
E_{gap}	1.76[52]	0.41[54]	eV
a_0	6.08[52]	5.935[55]	Å

Binding Energy

We start by studying the effect of lateral confinement on the binding energy of excitons and trions. For excitons, the binding energy is calculated as $E_b(X) = E_e + E_h - E(X)$, with $E(X)$ the the total exciton energy and $E_{e/h}$ that of an independent electron/hole. For the trion, it is defined as $E_b(X^{\pm}) = E(X) + E_{h/e} - E(X^{\pm})$, where $E(X^{\pm})$ is the total energy of the (positive or negative) trion. We take a NPL with one fixed lateral side (L_x = 20 nm) and vary the other side (L_y). The results are represented as blue squares in Figure 1. In the case of excitons, we also plot the binding energies obtained with a semi-analytic variational method,[13] blue circles in Fig. 1(a) and (b). The excellent agreement between the two methods validates the performance of the VQMC approach, which has the advantage of being computationally efficient for trions as well.

Figs. 1(a) and (b) show that the exciton binding energies in NPLs are large, which is a result of the quasi-2D geometry and the strong dielectric confinement. For CdSe NPLs, the values (225-265 meV) are consistent with previous theoretical estimates,[9,10,13,29] and experimental measurements.[56] In PbS NPLs, the binding energies (115-145 meV) exceed those calculated by Yang and Wise for quantum wells ($\sim$ 80 meV).[11] This is a consequence of the smaller thickness in our NPLs (L_z = 2 nm vs. L_z = 3 nm in their work), and suggests that recent progress in the synthesis of thin PbS NPLs[50,57,58] should facilitate the observation of robust excitonic effects. Also, our results evidence that PbS NPLs can benefit from a significant modulation of the binding energy with lateral confinement, starting at large lateral dimensions well above the PbS excitonic Bohr radius ($L_y < 30$ nm).

Figs.1(c) and (d) show the calculated trion binding energies for negative (blue squares) and positive (red squares) trions. The modulation of $E_b(X^{\pm})$ by lateral confinement is evident. In the case of CdSe, it enables binding energies greater than thermal energy at room temperature (24 meV) when $L_y < 15$ nm, which is consistent with Ref. 29 experiments. Even in the case of PbS, which has a large dielectric constant, the trion binding energies are one order of magnitude greater than those of epitaxial quantum wells.[59] For both materials

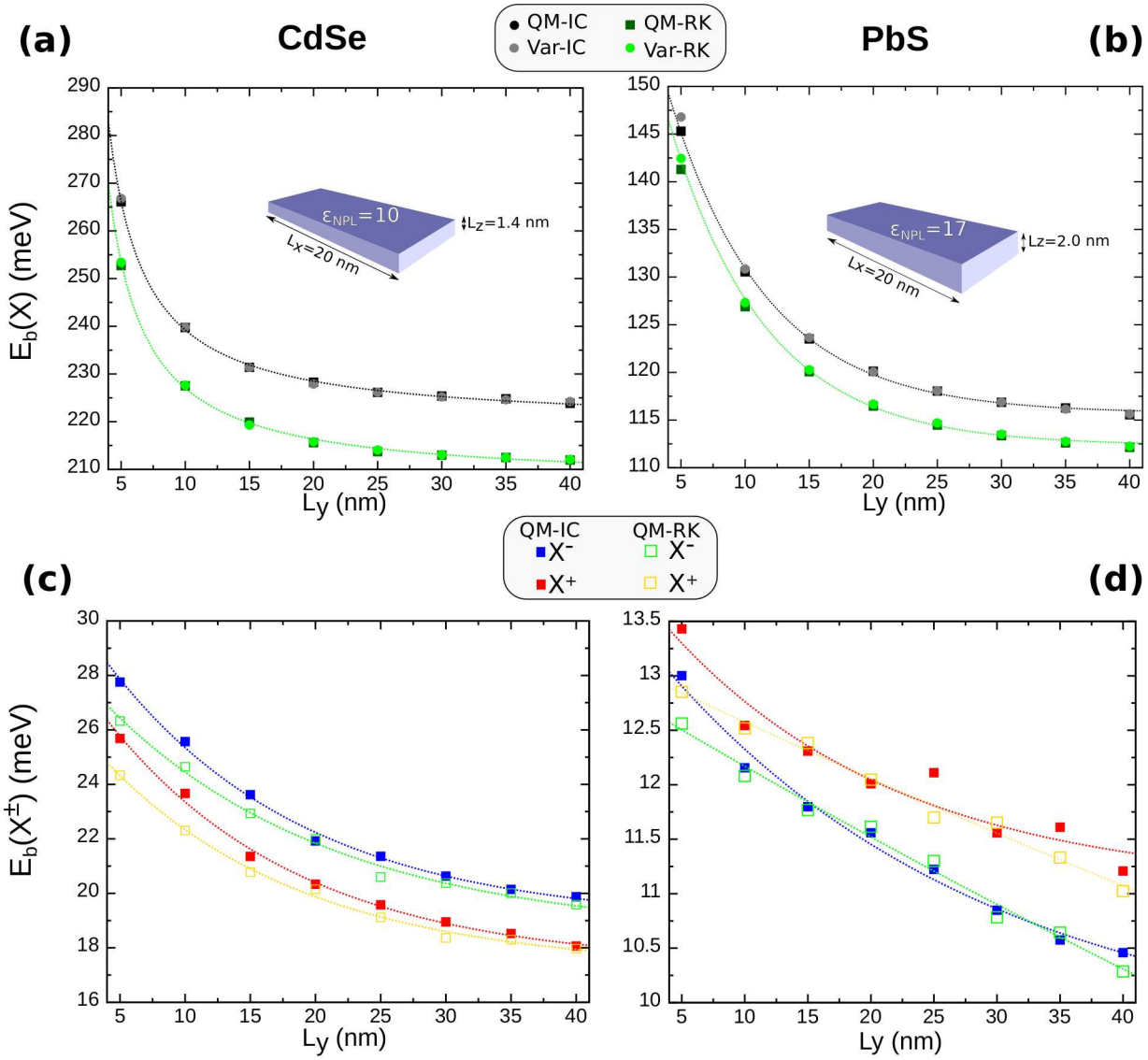

Figure 1: Binding energies as a function of lateral NPL confinement for: (a) CdSe exciton, (b) PbS exciton, (c) CdSe trions and (d) PbS trions. Squares are used for calculations using VQMC and circles for those using a semi-analytic variational calculation. IC and RK potentials describing dielectric confinement are also compared. Lines are guides to the eye. Fluctuations around them are due to the statistical nature of VQMC calculations. Insets: schematics of the NPLs under study.

and all dimensions under study, trions are bound ($E_b(X^{\pm}) > 0$), which should be seen in experiments as a redshifted emission when compared to excitons. This is a consequence of the strong Coulomb correlation, and is in contrast to small CdSe nanocrystals.[28,60]

Previous theoretical simulations of trions in NPLs using effective mass formalism intro-

duced dielectric effects in Coulomb interactions through a RK potential.[29] Although computationally this is a very efficient approximation, the potential was originally devised for strictly two-dimensional structures (graphene, transition metal dichalcogenides)[48] and its performance in colloidal NPLs, whose thickness can reach few nm, has not been tested. In Fig. 1 we compare the binding energies calculated with RK and IC potentials. For excitons, RK simultations (green squares in Fig. 1(a,b)) underestimate the binding energy by $5-10\%$ (cf. blue squares). For trions, however, RK and IC energies match within 1 meV difference. Since effective mass models are meant to provide qualitative and semi-quantitative estimates, these results support the use of the RK approximation to calculate binding energies in colloidal NPLs with typical (few monolayer) thicknesses. Nonetheless, for estimates of the emission energies, the RK potential must be complemented with self-energy corrections, as we show in the next section.

Modulation of dielectric confinement

The dielectric confinement exerted by the organic environment has been known to influence the electronic properties of excitons in colloidal NPLs since early studies.[9] The low dielectric constant of the organic medium enables strong Coulomb interactions, which give rise to large $E_b(X)$ values. The influence on negative trions was recently calculated in Ref. 29. It was concluded that with increasing dielectric mismatch between the NPL and the surroundings, $E_b(X^-)$ increases and its emission energy decreases, all because of the weaker screening of electron-hole attraction. The simulations however missed the self-energy correction Σ, which accounts for the effect of the polarization induced by the carriers on themselves.

In Fig. 2 we extend the study of dielectric confinement by comparing neutral excitons with both negative and positive trions in CdSe and PbS NPLs, as a function of the dielectric constant in the environment, ε_{out}. For all magnitudes under study, the reference energy is set to the case without dielectric mismatch, $\varepsilon_{out} = \varepsilon_{NPL}$. We consider the usual experimental regime, where the weak polarizability of the organic molecules surrounding the NPL imposes

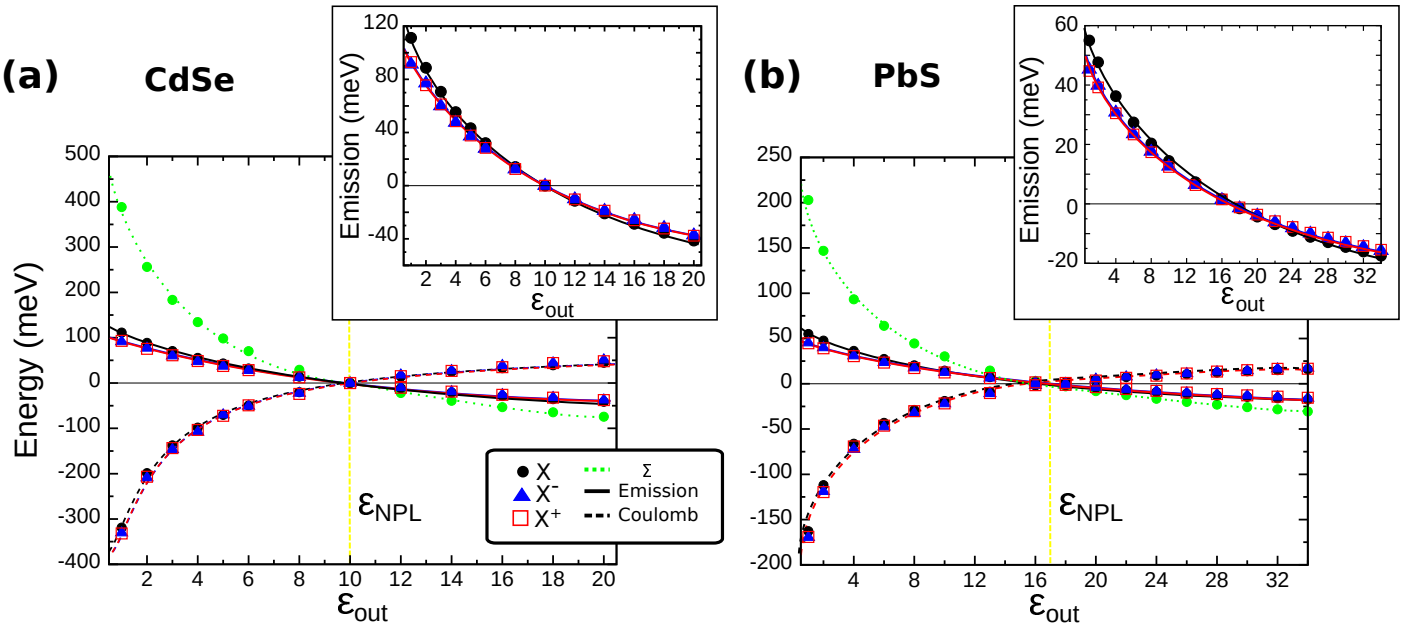

Figure 2: Shift of emission energy (solid line), net Coulomb energy (dashed line) and self-energy (dotted line) as a function of the dielectric constant in the environment in (a) CdSe NPL and (b) PbS NPL. All energies are referred to the $\varepsilon_{out} = \varepsilon_{NPL}$ case. Different symbols are used for excitons and trions. The NPL has 20×10 nm^2 area. The insets zoom in on the emission shift for excitons and trions, which result from the balance betwen Σ and the net Coulomb energy.

$\varepsilon_{out} \leq \varepsilon_{NPL}$, and also the opposite case, where $\varepsilon_{out} \geq \varepsilon_{NPL}$ (left and right sides of the vertical lines in the Figure). As can be seen, in spite of the Coulomb repulsions the behavior of X^- (triangles) and X^+ (squares) is generally similar to that of neutral excitons (dots).

When $\varepsilon_{out} \leq \varepsilon_{NPL}$, the net Coulomb interaction –i.e. the expectation value of attractions plus repulsions, not to be confused with the binding energy – (dashed line) becomes more and more attractive when ε_{out} decreases. The enhancement of the attractions is however compensated by an increase of the self-energy correction, Σ (dotted line). The latter term is greater than the former, which translates into an overall increase of the emission energy (solid line). Similar findings have been observed for excitons in PbS[11] and CdSe[13] NPLs. The extension to trions implies that the emission wavelength in such species can be also blueshifted by increasing the dielectric confinement. To better see the magnitude of this effect, insets are included in Fig. 2, which show that the blueshift can be few tens of meV large. Energy shifts due to dielectric confinement have been proposed to be the driving

mechanism for the formation of minibands in superlattices made of stacked NPLs.[61] The results in Fig. 2 indicate that such bands could be built not only from excitons but from trions as well.

When $\varepsilon_{out} \geq \varepsilon_{NPL}$, the sign of Σ and that of the Coulomb shifts reverse, which is a signature of the outer medium having now stronger polarizability than the NPL. This changes the sign of the charges induced on the dielectric interface, which scale as $q = (\varepsilon_{NPL} - \varepsilon_{out})/(\varepsilon_{NPL} + \varepsilon_{out})$.[47] Redshifts of up to a few tens of meV are then obtained in the emission (see insets in the figure). The dielectric effects are however weaker than for small ε_{out} values, which is easily understood from the scaling factor q.

The exact value of ε_{NPL} in small nanostructures is debatable, as the dielectric constant depends on the size of the crystal as well as on the frequency of the electric field within the exciton pair.[62] We have however checked that quantitatively similar results to those of Fig. 2 are obtained if one replaces the NPL dielectric constant by intermediate values between static and high-frequency limits, as suggested by studies in CdSe/CdS nanocrystals.[63] Again, this can be explained from the scaling factor q. Typical dielectric constants of metal chalcogenides are large (~ 10 for CdSe, ~ 17 for PbS). Moderate changes around these values have only little influence on q.

Balance between attractions and repulsions

To visualize the relative strength of attractions and repulsions of trions in NPLs, we decompose the energy of excitons and trions as:

$$E(X) = E_e + E_h + V_{eh}(X) + E_{gap}, \tag{7}$$

$$E(X^-) = 2E_e + E_h + 2V_{eh}(X^-) + V_{ee} + E_{gap}, \tag{8}$$

$$E(X^+) = E_e + 2E_h + 2V_{eh}(X^+) + V_{hh} + E_{gap}. \tag{9}$$

where E_e (E_h) is the expectation value of the electron (hole) single-particle terms in Hamiltonian (1), V_{eh} that of the electron-hole Coulomb term and V_{ee} (V_{hh}) that of electron-electron (hole-hole) Coulomb term.

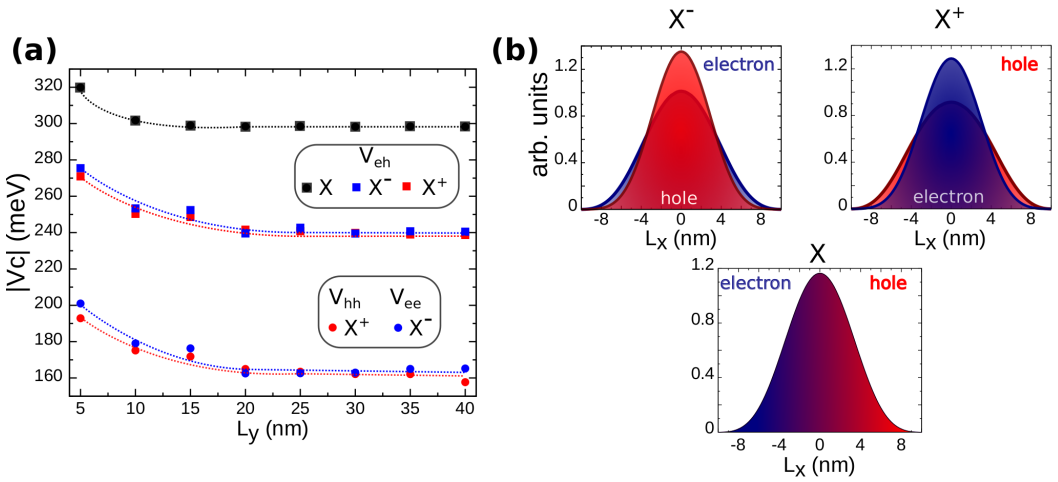

Figure 3: (a) Expectation value of the Coulomb terms of excitons and trions, and (b) charge densities along the x axis of the NPL in a CdSe NPL with $L_x = 20$ nm and $L_y = 5$ nm.

Figure 3(a) shows the calculated values of Coulomb energies CdSe NPLs with varying lateral size L_y. The electron-hole attraction of positive and negative trions is found to be similar, and clearly smaller than the attractions, $|V_{eh}(X^{\pm})| = 240 - 280$ meV, while $|V_{eh}(X)| = 300 - 320$ meV. The repulsions are also similar for X^- and X^+, but much smaller in energy ($160 - 200$ meV). Altogether, these findings indicate that the strong electronic correlations in colloidal NPLs make it possible for the trion to minimize repulsions and maximize attractions, as attractive and repulsive terms would be identical in a strongly confined dot.[64] This explains the sizable binding energies of trions reported in Fig. 1.

The role of electronic correlations in deforming the wave functions to stabilize excitonic states can be observed in Fig. 3(b). For a neutral exciton, electron and hole show identical charge densities despite the different masses. For trions, the repulsions between the carriers in excess (e.g. electrons in X^-) lead to somewhat larger delocalization, which reduces the electron-hole overlap substantially (note the smaller height of the charge density in the central region). These changes are reflected in the variational parameteres related to effective Bohr

radii: $r_B^X = 2.23$ nm for the exciton, $r_B^{X^-} = 2.53$ nm and $r_B^{X^+} = 2.98$ nm for the trions. The consequences on the optical properties properties are significant, as we show in the next section.

Emission spectra of CdSe NPLs

Having studied the general behavior of trions in NPLs, we next focus on the specific samples investigated in Ref. 29 and analyze their emission spectra. In Fig. 4(a) we compare the calculated emission energies of excitons and trions with those measured in the experiments. Our simulations overestimate the experimental values by ~ 10 meV, but the overall agreement is good and, importantly, it is achieved with no fitting parameter. The redshift of trions with respect to excitons ($20 - 30$ meV) is close to that of the experiments ($20 - 35$ meV), which shows we obtain consistent binding energies. The larger value as compared to CdSe/CdS/ZnS core/shell/shell NPLs ($E_b(X^-) = 10.5$ meV)[28] can be explained from: (i) the stronger dielectric confinement in core-only NPLs, which has significant influence on trion binding energies, as seen in the inset of Fig. 2(a), and (ii) the quasi-type-II band alignment of CdSe/CdS, which promotes electron delocalization and hence reduced Coulomb interaction with the hole.

Fig. 4(b) compares the recombination probability of excitons and trions. For the smallest NPLs (area 17×6 nm^2), the probability is similar in all species. This is in spite of trions having no spin-forbidden (dark) optical recombination channels, as opposed to neutral excitons, for which half of the states are dark (notice the 1/2 factor in Eq. (5)). The reason is that the repulsions in trions reduce the electron-hole overlap, as seen in the charge densities of Fig. 3(b). Consequently, the ratio of the (spin-independent) trion-to-exciton oscillator strength is about 0.45 (see leftmost part of Fig. 4(c)). With increasing lateral dimensions of the NPL, the giant oscillator strength effect boosts the recombination probability of X, which scales roughly linearly with the area.[65,66] This is not observed in trions instead. For $X^{\pm}$, the increase is much weaker and saturates for large areas (> 400 nm^2). The resulting oscillator

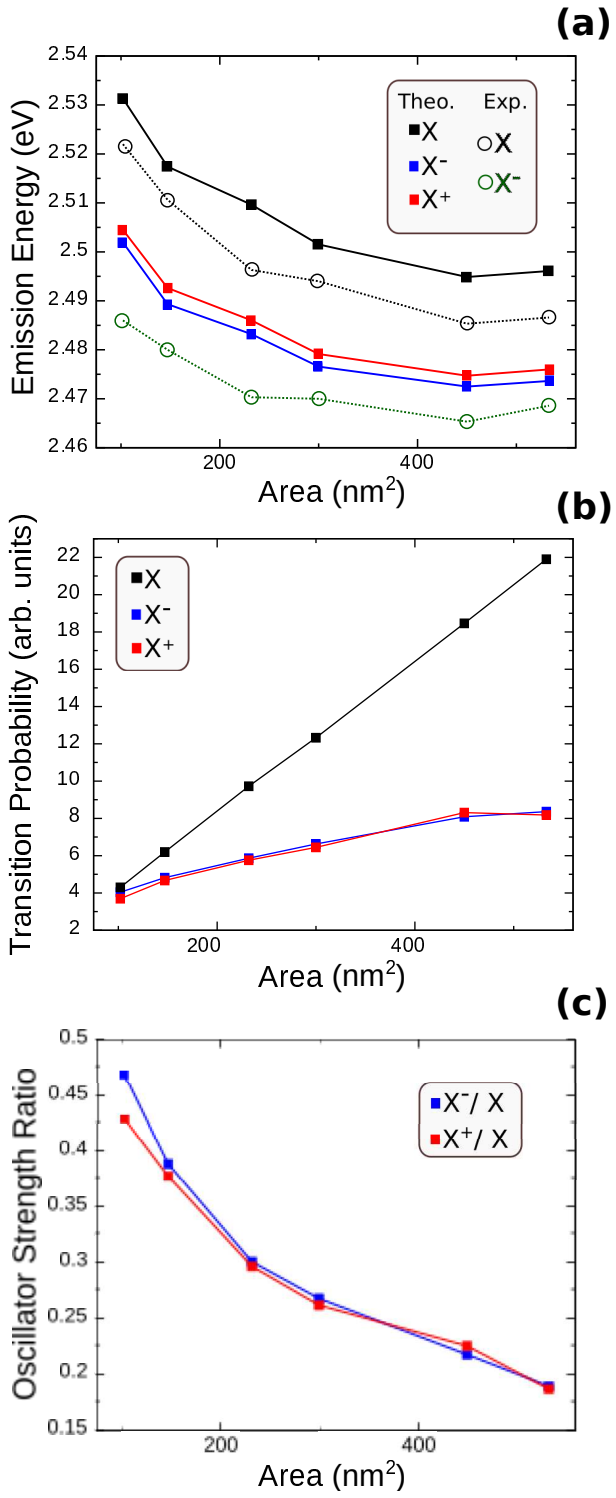

Figure 4: Analysis of emission properties for the CdSe NPLs of Ref. 29. (a) Comparison of theoretical and experimental emission energies. (b) Calculated recombination probability. (c) Calculated ratio between oscillator strengths of trions and excitons. We include positive trions for completeness.

strength for large area NPLs is then smaller than that of excitons. For the larger NPLs under consideration the ratio is ~ 0.2, (area 41×13 nm^2, see rightmost part of Fig. 4(c)).

The oscillator strength ratios we obtain are in between those reported for CdSe/CdS/ZnS NPLs,[28] which are close to unity, and those calculated for CdSe NPLs in earlier studies, which range between 0.12 and 0.04.[29] The smaller values as compared to CdSe/CdS/ZnS can be interpreted from the absence of shells, which translates into larger dielectric mismatch.[15] This gives rise to stronger electronic correlations, which in turn permit shaping wave functions to minimize repulsions. As for the larger values compared to Ref. 29 calculations, since both theoretical models rely on effective mass Hamiltonians, describe dielectric confinement with methods of similar outcome (Fig. 1), and provide good estimates of the experimentally observed emission and binding energies, the differences must be ascribed to the inclusion of many-body interactions in the wave function. Since VQMC calculations treat attractions and repulsions on equal footing, the resulting charge distribution of trions is less likely to overestimate the Bohr radius as compared to CI calculations. In this sense, it is not surprising that we obtain somewhat larger oscillator strengths.

The saturation of the trion transition probability beyond 400 nm^2 in Fig. 4(b) is also in contrast to the linear increase in the calculations of Ref. 29. We note that our result is consistent with the expected behavior as one approaches the quantum well limit. In the formation of a (say, negative) trion, the initial electron is originally delocalized over the NPL volume, but it ends up being localized in the volume of the photocreated trion. This localization leads to a reduction factor $1/A$ in the oscillator strength as compared to the exciton, with $A = L_x L_y$ the NPL area – see for instance Eq. (13.51) in Ref. 67–. Since for the exciton, $|\langle 0|\delta_{\mathbf{r_e},\mathbf{r_h}}|\Psi_X\rangle|^2 \propto A$,[65,66] for the trion $\left|\langle \Psi_e|\delta_{\mathbf{r_{e_2}},\mathbf{r_{h_1}}}|\Psi_{X^-}\rangle\right|^2 \propto A^0$. Thus, for large NPLs we observe the 2D asymptotic behavior not only in the trion emission energies but also in its oscillator strength.

We close this section with a few practical considerations. In general, transition probabilities depend on the oscillator strength and, for the neutral exciton, on the relative occupation

of dark and bright states. The emission rates presented in Fig. 4b assume equipopulated dark and bright neutral exciton states (as is the case at temperatures above 100 K[25]). If temperatures were lower, the thermal occupation of bright excitons would decrease and so would the 1/2 factor in Eq. (5). Trions may then display faster emission rates as compared to excitons. Still, because of the oscillator strength behavior (Fig. 4(c)), increasing the NPL area would tend to to invert this trend. Also, we have assumed ideal NPLs where excitons and trions move freely all over the area. However, state-of-the-art NPLs often suffer from surface defects and interaction with phonon modes whose effect is to localize excitons within narrower areas.[68] This limits the giant oscillator strength effect, such that the ratio between trion and exciton oscillator strengths is more likely to stay in the left-most part of Fig. 4(c). Clear manifestations of the giant oscillator strength up to large areas have been however reported in some experiments with CdSe NPLs.[66]

Conclusions

We have compared exciton and trion optoelectronic properties in NPLs of CdSe and PbS. The pronounced electronic correlations in colloidal NPLs allow trions to reduce Coulomb repulsions while keeping attractions strong. A few signatures of this are observed. First, both negative and positive trions are redshifted with respect to the exciton, with binding energies that exceed room temperature thermal energy in the case of CdSe with narrow lateral dimensions. Second, contrary to excitons, the trion oscillator strength does not increase linearly with the NPL area, as the giant oscillator strength effect is significantly suppressed and vanishes for large areas.

Our calculations show that the description of dielectric confinement with simple 2D Rytova-Keldysh potentials provide similar estimates of binding energies to those of (fully 3D) image charge potentials in colloidal NPLs with typical (few-nm) thicknesses. However, they also evidence the need to add self-energy corrections so as to predict the right dependence

of emission energy on the dielectric mismatch. These results are of interest for the design of optoelectronic devices using homostructured NPLs populated with trions.

Acknowledgement

We are grateful to Sabrine Ayari and Sihem Jaziri for discussions. Finacial support from MINECO project CTQ2017-83781-P (JP,JIC), the European Research Council (ERC) via Consolidator Grant 724424-No-LIMIT (D.M-P., I. M.-S.) and Generalitat Valenciana via Prometeo Grant Q-Devices (Prometeo/2018/098) is gratefully acknowledged.

References

(1) Chen, Z.; Nadal, B.; Mahler, B.; Aubin, H.; Dubertret, B. Quasi-2D Colloidal Semiconductor Nanoplatelets for Narrow Electroluminescence. *Advanced Functional Materials* **2014**, *24*, 295–302.

(2) Diroll, B. T. Colloidal quantum wells for optoelectronic devices. *Journal of Materials Chemistry C* **2020**, *8*, 10628–10640.

(3) Dutta, A.; Medda, A.; Patra, A. Recent Advances and Perspectives on Colloidal Semiconductor Nanoplatelets for Optoelectronic Applications. *The Journal of Physical Chemistry C* **2021**, *125*, 20–30.

(4) Nasilowski, M.; Mahler, B.; Lhuillier, E.; Ithurria, S.; Dubertret, B. Two-dimensional colloidal nanocrystals. *Chemical reviews* **2016**, *116*, 10934–10982.

(5) Zhang, J.; Sun, Y.; Ye, S.; Song, J.; Qu, J. Heterostructures in Two-Dimensional CdSe Nanoplatelets: Synthesis, Optical Properties, and Applications. *Chemistry of Materials* **2020**, *32*, 9490–9507.

(6) Pun, A. B.; Mazzotti, S.; Mule, A. S.; Norris, D. J. Understanding Discrete Growth in Semiconductor Nanocrystals: Nanoplatelets and Magic-Sized Clusters. *Accounts of Chemical Research* **2021**, 743–748.

(7) Min, Y.; Im, E.; Hwang, G.-T.; Kim, J.-W.; Ahn, C.-W.; Choi, J.-J.; Hahn, B.-D.; Choi, J.-H.; Yoon, W.-H.; Park, D.-S. Heterostructures in two-dimensional colloidal metal chalcogenides: Synthetic fundamentals and applications. *Nano Research* **2019**, *12*, 1750–1769.

(8) Ithurria, S.; Tessier, M.; Mahler, B.; Lobo, R.; Dubertret, B.; Efros, A. L. Colloidal nanoplatelets with two-dimensional electronic structure. *Nature materials* **2011**, *10*, 936–941.

(9) Achtstein, A. W.; Schliwa, A.; Prudnikau, A.; Hardzei, M.; Artemyev, M. V.; Thomsen, C.; Woggon, U. Electronic structure and exciton–phonon interaction in two-dimensional colloidal CdSe nanosheets. *Nano letters* **2012**, *12*, 3151–3157.

(10) Benchamekh, R.; Gippius, N. A.; Even, J.; Nestoklon, M. O.; Jancu, J.-M.; Ithurria, S.; Dubertret, B.; Efros, A. L.; Voisin, P. Tight-binding calculations of image-charge effects in colloidal nanoscale platelets of CdSe. *Phys. Rev. B* **2014**, *89*, 035307.

(11) Yang, J.; Wise, F. Electronic states of lead-salt nanosheets. *The Journal of Physical Chemistry C* **2015**, *119*, 26809–26816.

(12) Bose, S.; Song, Z.; Fan, W. J.; Zhang, D. H. Effect of lateral size and thickness on the electronic structure and optical properties of quasi two-dimensional CdSe and CdS nanoplatelets. *Journal of Applied Physics* **2016**, *119*, 143107.

(13) Rajadell, F.; Climente, J. I.; Planelles, J. Excitons in core-only, core-shell and core-crown CdSe nanoplatelets: Interplay between in-plane electron-hole correlation, spatial confinement, and dielectric confinement. *Physical Review B* **2017**, *96*, 035307.

(14) Richter, M. Nanoplatelets as material system between strong confinement and weak confinement. *Physical Review Materials* **2017**, *1*, 016001.

(15) Polovitsyn, A.; Dang, Z.; Movilla, J. L.; Martín-García, B.; Khan, A. H.; Bertrand, G. H.; Brescia, R.; Moreels, I. Synthesis of air-stable CdSe/ZnS core–shell nanoplatelets with tunable emission wavelength. *Chemistry of Materials* **2017**, *29*, 5671–5680.

(16) Chu, A.; Livache, C.; Ithurria, S.; Lhuillier, E. Electronic structure robustness and design rules for 2D colloidal heterostructures. *Journal of Applied Physics* **2018**, *123*, 035701.

(17) Achtstein, A. W.; Marquardt, O.; Scott, R.; Ibrahim, M.; Riedl, T.; Prudnikau, A. V.; Antanovich, A.; Owschimikow, N.; Lindner, J. K.; Artemyev, M. Impact of shell growth on recombination dynamics and exciton–phonon interaction in CdSe–CdS core–shell nanoplatelets. *ACS nano* **2018**, *12*, 9476–9483.

(18) Specht, J. F.; Scott, R.; Castro, M. C.; Christodoulou, S.; Bertrand, G. H.; Prudnikau, A. V.; Antanovich, A.; Siebbeles, L. D.; Owschimikow, N.; Moreels, I. Size-dependent exciton substructure in CdSe nanoplatelets and its relation to photoluminescence dynamics. *Nanoscale* **2019**, *11*, 12230–12241.

(19) Llusar, J.; Planelles, J.; Climente, J. I. Strain in lattice-mismatched CdSe-based core/shell nanoplatelets. *The Journal of Physical Chemistry C* **2019**, *123*, 21299–21306.

(20) Steinmetz, V.; Climente, J. I.; Pandya, R.; Planelles, J.; Margaillan, F.; Puttisong, Y.; Dufour, M.; Ithurria, S.; Sharma, A.; Lakhwani, G. Emission State Structure and Linewidth Broadening Mechanisms in Type-II CdSe/CdTe Core–Crown Nanoplatelets: A Combined Theoretical–Single Nanocrystal Optical Study. *The Journal of Physical Chemistry C* **2020**, *124*, 17352–17363.

(21) Macias-Pinilla, D. F.; Echeverría-Arrondo, C.; Gualdrón Reyes, A. F.; Agouram, S.; Muñoz-Sanjosé, V.; Planelles, J.; Mora-Seró, I.; Climente, J. I. Morphology and Band Structure of Orthorhombic PbS Nanoplatelets: An Indirect Band Gap Material. *Chemistry of Materials* **2021**, *33*, 420–429.

(22) Greenwood, A. R.; Mazzotti, S.; Norris, D. J.; Galli, G. Determining the Structure–Property Relationships of Quasi-Two-Dimensional Semiconductor Nanoplatelets. *The Journal of Physical Chemistry C* **2021**, *125*, 4820–4827.

(23) Lorenzon, M.; Christodoulou, S.; Vaccaro, G.; Pedrini, J.; Meinardi, F.; Moreels, I.; Brovelli, S. Reversed oxygen sensing using colloidal quantum wells towards highly emissive photoresponsive varnishes. *Nature Communications* **2015**, *6*, 6434.

(24) Yu, J.; Zhang, C.; Pang, G.; Sun, X. W.; Chen, R. Effect of lateral size and surface passivation on the near-band-edge excitonic emission from quasi-two-dimensional CdSe nanoplatelets. *ACS applied materials & interfaces* **2019**, *11*, 41821–41827.

(25) Shornikova, E. V.; Yakovlev, D. R.; Biadala, L.; Crooker, S. A.; Belykh, V. V.; Kochiev, M. V.; Kuntzmann, A.; Nasilowski, M.; Dubertret, B.; Bayer, M. Negatively Charged Excitons in CdSe Nanoplatelets. *Nano Letters* **2020**, *20*, 1370–1377, PMID: 31960677.

(26) Antolinez, F. V.; Rabouw, F. T.; Rossinelli, A. A.; Cui, J.; Norris, D. J. Observation of electron shakeup in CdSe/CdS core/shell nanoplatelets. *Nano letters* **2019**, *19*, 8495–8502.

(27) Antolinez, F. V.; Rabouw, F. T.; Rossinelli, A. A.; Keitel, R. C.; Cocina, A.; Becker, M. A.; Norris, D. J. Trion emission dominates the low-temperature photoluminescence of CdSe nanoplatelets. *Nano Letters* **2020**, *20*, 5814–5820.

(28) Peng, L.; Otten, M.; Hazarika, A.; Coropceanu, I.; Cygorek, M.; Wiederrecht, G. P.;

Hawrylak, P.; Talapin, D. V.; Ma, X. Bright trion emission from semiconductor nanoplatelets. *Physical Review Materials* **2020**, *4*, 056006.

(29) Ayari, S.; Quick, M. T.; Owschimikow, N.; Christodoulou, S.; Bertrand, G. H.; Artemyev, M.; Moreels, I.; Woggon, U.; Jaziri, S.; Achtstein, A. W. Tuning trion binding energy and oscillator strength in a laterally finite 2D system: CdSe nanoplatelets as a model system for trion properties. *Nanoscale* **2020**, *12*, 14448–14458.

(30) Kunneman, L. T.; Tessier, M. D.; Heuclin, H.; Dubertret, B.; Aulin, Y. V.; Grozema, F. C.; Schins, J. M.; Siebbeles, L. D. Bimolecular Auger recombination of electron–hole pairs in two-dimensional CdSe and CdSe/CdZnS core/shell nanoplatelets. *The Journal of Physical Chemistry Letters* **2013**, *4*, 3574–3578.

(31) Baghani, E.; O'Leary, S. K.; Fedin, I.; Talapin, D. V.; Pelton, M. Auger-limited carrier recombination and relaxation in CdSe colloidal quantum wells. *The journal of physical chemistry letters* **2015**, *6*, 1032–1036.

(32) Li, Q.; Lian, T. Area-and thickness-dependent biexciton Auger recombination in colloidal CdSe nanoplatelets: breaking the "Universal Volume Scaling Law". *Nano letters* **2017**, *17*, 3152–3158.

(33) Philbin, J. P.; Brumberg, A.; Diroll, B. T.; Cho, W.; Talapin, D. V.; Schaller, R. D.; Rabani, E. Area and thickness dependence of Auger recombination in nanoplatelets. *The Journal of Chemical Physics* **2020**, *153*, 054104.

(34) Löbl, M. C.; Spinnler, C.; Javadi, A.; Zhai, L.; Nguyen, G. N.; Ritzmann, J.; Midolo, L.; Lodahl, P.; Wieck, A. D.; Ludwig, A. Radiative Auger process in the single-photon limit. *Nature Nanotechnology* **2020**, *15*, 558–562.

(35) Llusar, J.; Climente, J. I. Nature and Control of Shakeup Processes in Colloidal Nanoplatelets. *ACS Photonics* **2020**, *7*, 3086–3095.

(36) Brumberg, A.; Harvey, S. M.; Philbin, J. P.; Diroll, B. T.; Lee, B.; Crooker, S. A.; Wasielewski, M. R.; Rabani, E.; Schaller, R. D. Determination of the In-Plane Exciton Radius in 2D CdSe Nanoplatelets via Magneto-optical Spectroscopy. *ACS nano* **2019**, *13*, 8589–8596.

(37) Planelles, J. Simple correlated wave-function for excitons in 0D, quasi-1D and quasi-2D quantum dots. *Theoretical Chemistry Accounts* **2017**, *136*, 1–16.

(38) Rontani, M.; Eriksson, G.; Åberg, S.; Reimann, S. M. On the renormalization of contact interactions for the configuration-interaction method in two-dimensions. *Journal of Physics B: Atomic, Molecular and Optical Physics* **2017**, *50*, 065301.

(39) Planelles, J.; Climente, J. I. A simple variational quantum Monte Carlo-effective mass approach for excitons and trions in quantum dots. *Computer Physics Communications* **2021**, *261*, 107782.

(40) Carey, G. H.; Abdelhady, A. L.; Ning, Z.; Thon, S. M.; Bakr, O. M.; Sargent, E. H. Colloidal quantum dot solar cells. *Chemical reviews* **2015**, *115*, 12732–12763.

(41) Sánchez-Godoy, H. E.; Erazo, E. A.; Gualdrón-Reyes, A. F.; Khan, A. H.; Agouram, S.; Barea, E. M.; Rodriguez, R. A.; Zarazúa, I.; Ortiz, P.; Cortés, M. T. et al. Preferred Growth Direction by PbS Nanoplatelets Preserves Perovskite Infrared Light Harvesting for Stable, Reproducible, and Efficient Solar Cells. *Advanced Energy Materials* **2020**, *10*, 2002422.

(42) De Iacovo, A.; Venettacci, C.; Colace, L.; Scopa, L.; Foglia, S. PbS Colloidal Quantum Dot Photodetectors operating in the near infrared. *Scientific Reports* **2016**, *6*, 37913.

(43) Sanchez, R. S.; Binetti, E.; Torre, J. A.; Garcia-Belmonte, G.; Striccoli, M.; Mora-Sero, I. All solution processed low turn-on voltage near infrared LEDs based on core–shell PbS–CdS quantum dots with inverted device structure. *Nanoscale* **2014**, *6*, 8551–8555.

(44) Fan, F.; Kanjanaboos, P.; Saravanapavanantham, M.; Beauregard, E.; Ingram, G.; Yassitepe, E.; Adachi, M. M.; Voznyy, O.; Johnston, A. K.; Walters, G. et al. Colloidal CdSe1–x S x Nanoplatelets with Narrow and Continuously-Tunable Electroluminescence. *Nano letters* **2015**, *15*, 4611–4615.

(45) van Der Bok, J. C.; Dekker, D. M.; Peerlings, M. L.; Salzmann, B. B.; Meijerink, A. Luminescence Line Broadening of CdSe Nanoplatelets and Quantum Dots for Application in w-LEDs. *The Journal of Physical Chemistry C* **2020**, *124*, 12153–12160.

(46) Guzelturk, B.; Kelestemur, Y.; Olutas, M.; Delikanli, S.; Demir, H. V. Amplified spontaneous emission and lasing in colloidal nanoplatelets. *ACS nano* **2014**, *8*, 6599–6605.

(47) Kumagai, M.; Takagahara, T. Excitonic and nonlinear-optical properties of dielectric quantum-well structures. *Physical Review B* **1989**, *40*, 12359.

(48) Cudazzo, P.; Tokatly, I. V.; Rubio, A. Dielectric screening in two-dimensional insulators: Implications for excitonic and impurity states in graphane. *Physical Review B* **2011**, *84*, 085406.

(49) Jacak, L.; Hawrylak, P.; Wojs, A. *Quantum Dots*; Springer, 1998.

(50) Antu, A. D.; Jiang, Z.; Premathilka, S. M.; Tang, Y.; Hu, J.; Roy, A.; Sun, L. Bright colloidal PbS nanoribbons. *Chemistry of Materials* **2018**, *30*, 3697–3703.

(51) Lüdde, K. Das dielektrische und refraktodensimetrische Verhalten flüssiger Fette beim Altern. *Fette, Seifen, Anstrichmittel* **1959**, *61*, 1156–1163.

(52) Adachi, S. *Handbook on physical properties of semiconductors*; Springer Science & Business Media, 2004; Vol. 2.

(53) Gupta, B.; Kumar, V. Analysis of effective compressibilities in PbS, PbSe, PbTe and SnTe. *Solid State Communications* **1983**, *45*, 745–747.

(54) Kang, I.; Wise, F. W. Electronic structure and optical properties of PbS and PbSe quantum dots. *JOSA B* **1997**, *14*, 1632–1646.

(55) Hoda, S. N.; Chang, L. L. Phase relations in the systems PbS-Ag2S-Sb2S3 and PbS-Ag2S-Bi2S3. *American Mineralogist: Journal of Earth and Planetary Materials* **1975**, *60*, 621–633.

(56) Zelewski, S. J.; Nawrot, K. C.; Zak, A.; Gladysiewicz, M.; Nyk, M.; Kudrawiec, R. Exciton binding energy of two-dimensional highly luminescent colloidal nanostructures determined from combined optical and photoacoustic spectroscopies. *The journal of physical chemistry letters* **2019**, *10*, 3459–3464.

(57) Khan, A. H.; Brescia, R.; Polovitsyn, A.; Angeloni, I.; Martín-García, B.; Moreels, I. Near-Infrared emitting colloidal PbS nanoplatelets: lateral size control and optical spectroscopy. *Chemistry of Materials* **2017**, *29*, 2883–2889.

(58) Akkerman, Q. A.; Martín-García, B.; Buha, J.; Almeida, G.; Toso, S.; Marras, S.; Bonaccorso, F.; Petralanda, U.; Infante, I.; Manna, L. Ultrathin Orthorhombic PbS Nanosheets. *Chemistry of Materials* **2019**, *31*, 8145–8153.

(59) Esser, A.; Runge, E.; Zimmermann, R.; Langbein, W. Photoluminescence and radiative lifetime of trions in GaAs quantum wells. *Physical Review B* **2000**, *62*, 8232.

(60) Califano, M.; Franceschetti, A.; Zunger, A. Lifetime and polarization of the radiative decay of excitons, biexcitons, and trions in CdSe nanocrystal quantum dots. *Physical Review B* **2007**, *75*, 115401.

(61) Movilla, J. L.; Planelles, J.; Climente, J. I. Dielectric Confinement Enables Molecular Coupling in Stacked Colloidal Nanoplatelets. *J. Phys. Chem. Lett.* **2020**, *11*, 3294–3300.

(62) Rodina, A.; Efros, A. L. Effect of dielectric confinement on optical properties of colloidal nanostructures. *Journal of Experimental and Theoretical Physics* **2016**, *122*, 554–566.

(63) Angeloni, I.; Raja, W.; Brescia, R.; Polovitsyn, A.; De Donato, F.; Canepa, M.; Bertoni, G.; Proietti Zaccaria, R.; Moreels, I. Disentangling the Role of Shape, Ligands, and Dielectric Constants in the Absorption Properties of Colloidal CdSe/CdS Nanocrystals. *ACS Photonics* **2016**, *3*, 58–67.

(64) Lelong, P.; Bastard, G. Binding energies of excitons and charged excitons in GaAsGa (In) As quantum dots. *Solid state communications* **1996**, *98*, 819–823.

(65) Feldmann, J.; Peter, G.; Göbel, E.; Dawson, P.; Moore, K.; Foxon, C.; Elliott, R. Linewidth dependence of radiative exciton lifetimes in quantum wells. *Physical review letters* **1987**, *59*, 2337.

(66) Planelles, J.; Achtstein, A. W.; Scott, R.; Owschimikow, N.; Woggon, U.; Climente, J. I. Tuning intraband and interband transition rates via excitonic correlation in low-dimensional semiconductors. *ACS Photonics* **2018**, *5*, 3680–3688.

(67) Combescot, M.; Shiau, S.-Y. *Excitons and Cooper pairs: two composite bosons in many-body physics*; Oxford University Press, 2015.

(68) Geiregat, P.; Rodá, C.; Tanghe, I.; Singh, S.; Di Giacomo, A.; Lebrun, D.; Grimaldi, G.; Maes, J.; Van Thourhout, D.; Moreels, I. et al. Localization-limited exciton oscillator strength in colloidal CdSe nanoplatelets revealed by the optically induced stark effect. *Light: Science & Applications* **2021**, *10*, 1–11.

Graphical TOC Entry